RNA-multi-omics in single cells reveal rhythmical RNA reshaping during human and mouse oocyte maturation

Huan Yao[1,2,4,5], Danru Zhang[3,4], Haixia Jing[1,4], Yanjie Guo[1,4], Yan Liu[1], Shengnan Wang[1], Shenli Yuan[2,5], Gang Lu[2,5], Yingpu Sun[1,5]

[1]Center for Reproductive Medicine, Henan Key Laboratory of Reproduction and Genetics, The First Affiliated Hospital of Zhengzhou University, Zhengzhou, China

[2]School of Biomedical Sciences. The Chinese University of Hong Kong

[3]CAS Key Laboratory of Genomic and Precision Medicine, Collaborative Innovation Center of Genetics and Development, College of Future Technology, Beijing Institute of Genomics, Chinese Academy of Sciences and China National Center for Bioinformation

[4]These authors contributed equally: Huan Yao, Danru Zhang, Haixia Jing, Yanjie Guo

[5]Lead contact

*e-mail: huanyao@cuhk.edu.hk, yuan1920946414@126.com, lugang@cuhk.edu.hk, syp2008@vip.sina.com

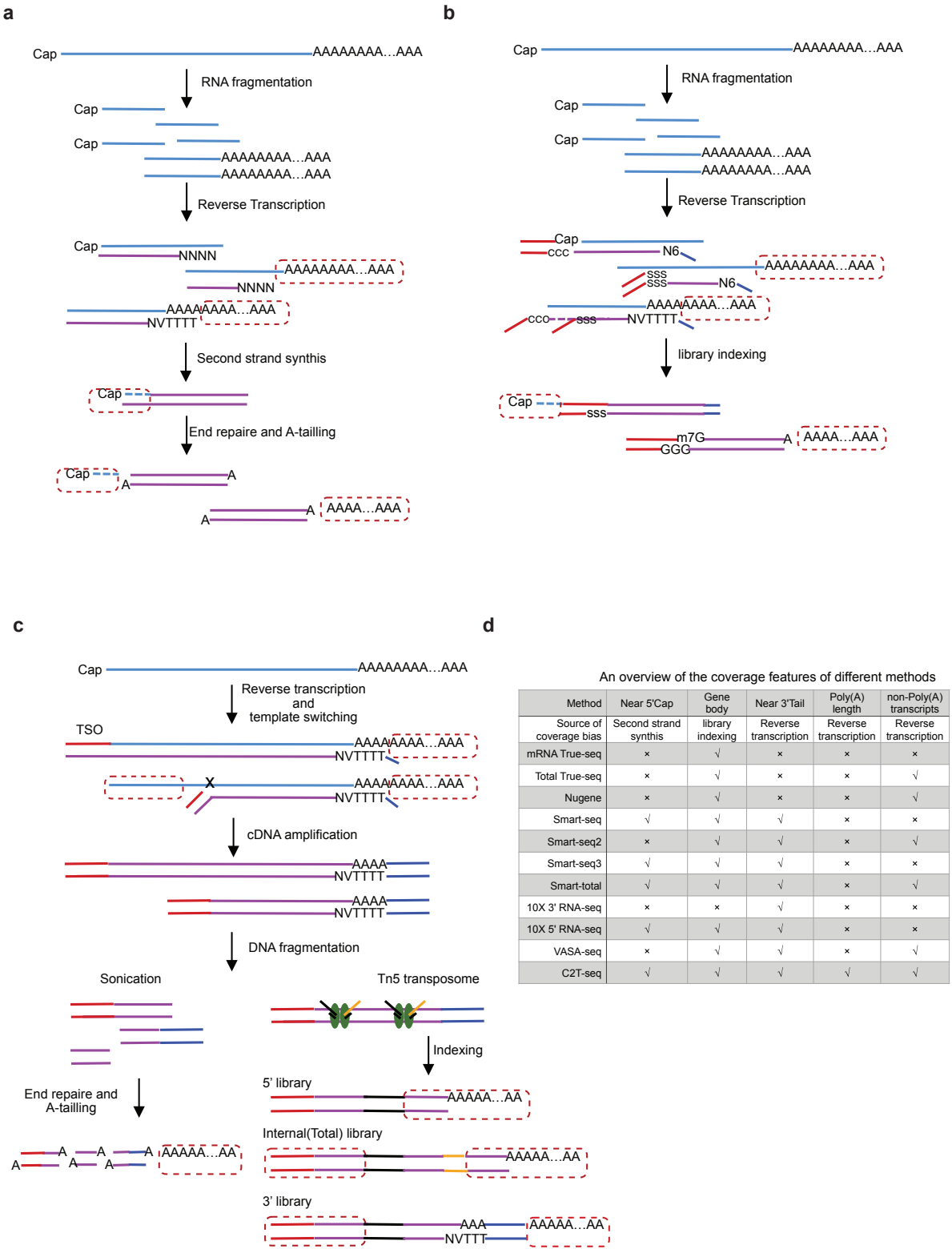

d

An overview of the coverage features of different methods

Method	Near 5'Cap	Gene body	Near 3'Tail	Poly(A) length	non-Poly(A) transcripts
Source of coverage bias	Second strand synthis	library indexing	Reverse transcription	Reverse transcription	Reverse transcription
mRNA True-seq	×	√	×	×	×
Total True-seq	×	√	×	×	√
Nugene	×	√	×	×	√
Smart-seq	√	√	√	×	×
Smart-seq2	×	√	√	×	√
Smart-seq3	√	√	√	×	×
Smart-total	√	√	√	×	√
10X 3' RNA-seq	×	×	√	×	×
10X 5' RNA-seq	√	√	√	×	×
VASA-seq	×	√	√	×	√
C2T-seq	√	√	√	√	√

Figure 1| RNA muti-omics analysis using C2T-App. a-c Schematic diagram showing the the missing RNA elements during standard RNA-seq protocol (**a**), SMART-total RNA-seq protocol (**b**), and SMART-seq protocol (**c**), the missing RNA elements are marked with a red dashed box. **d** A summary of the coverage bias of some popular existing RNA-seq methods and C2T-seq.

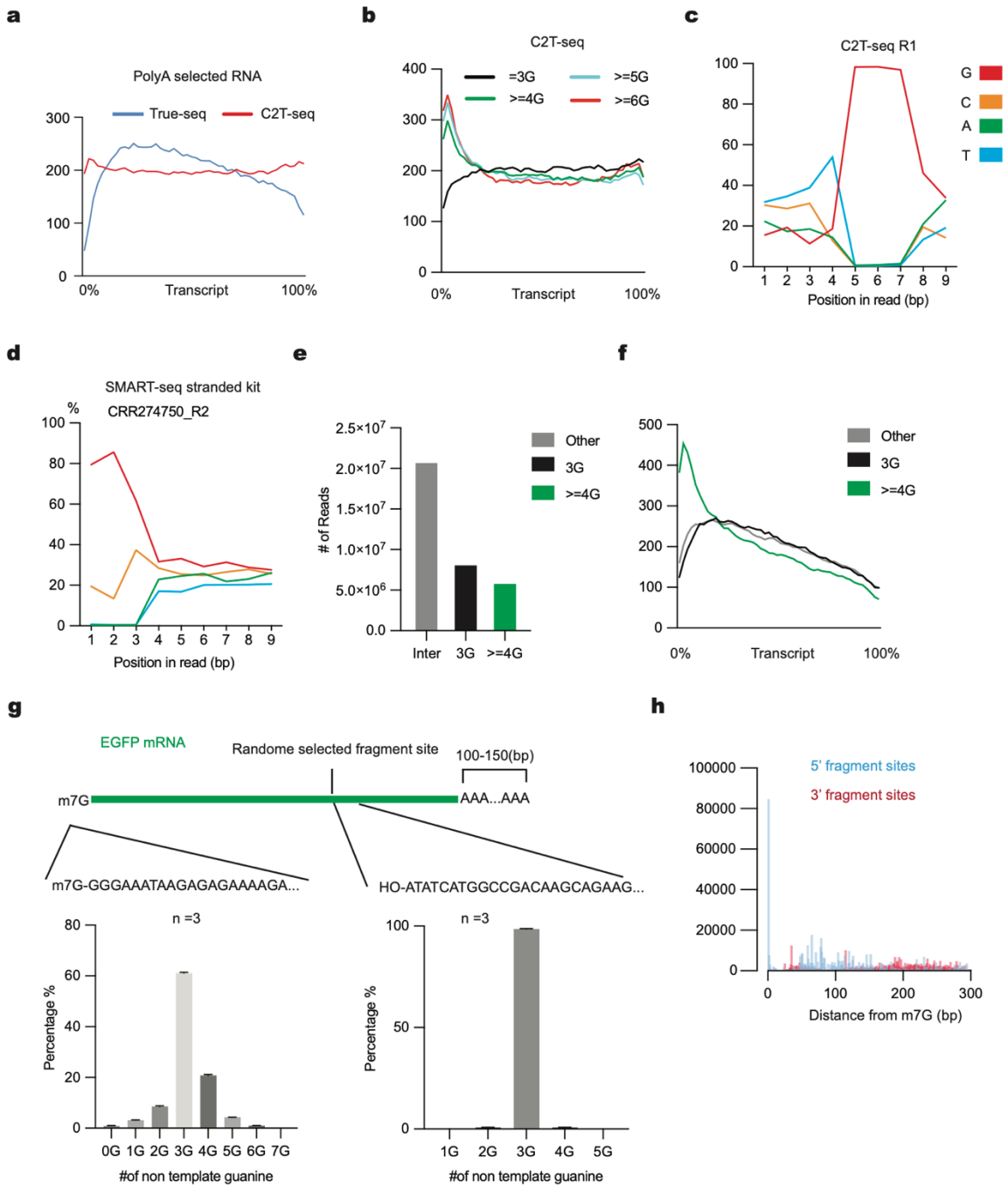

Figure 2| Cap and Tail analysis of C2T-seq data using C2T-App. a Meta-gene plot showing the coverage distribution of libraries constructed using True-seq kit (TAKARA) and C2T-seq using poly(A) selected mRNA. **b** Meta-gene plot showing the coverage of different classes of reads, the reads are classified using the R2 reads of C2T-seq libraries. **c** The first nine bases of the R1 data of C2T-seq libraries. **d** The first nine bases of the R2 data of libraries constructed using SMART-

total kit (TAKARA). **e** Bar plot showing the proportion of different reads classes in libraries constructed using SMART-total kit. **f** Meta-gene plot showing the coverage of different classes of reads, the reads are classified using the R1 reads of SMART-total libraries. **g** A commercial EGFP mRNA with m^7G Cap and 100-150 bp poly(A) tail was used to confirm the different cDNA end of 5' m^7G RNA and OH/Phos 5' structure RNA (upper). A random internal site was selected for further comparison (n=3). Bar plot showing the number of G in the cDNA end of 5' m^7G RNA and OH/Phos 5' structure RNA (lower). **h** Bar plot showing the distribution of the 5' terminal (R1) and 3' terminal sites (R2) mapped around the EGFP mRNA m^7G cap.

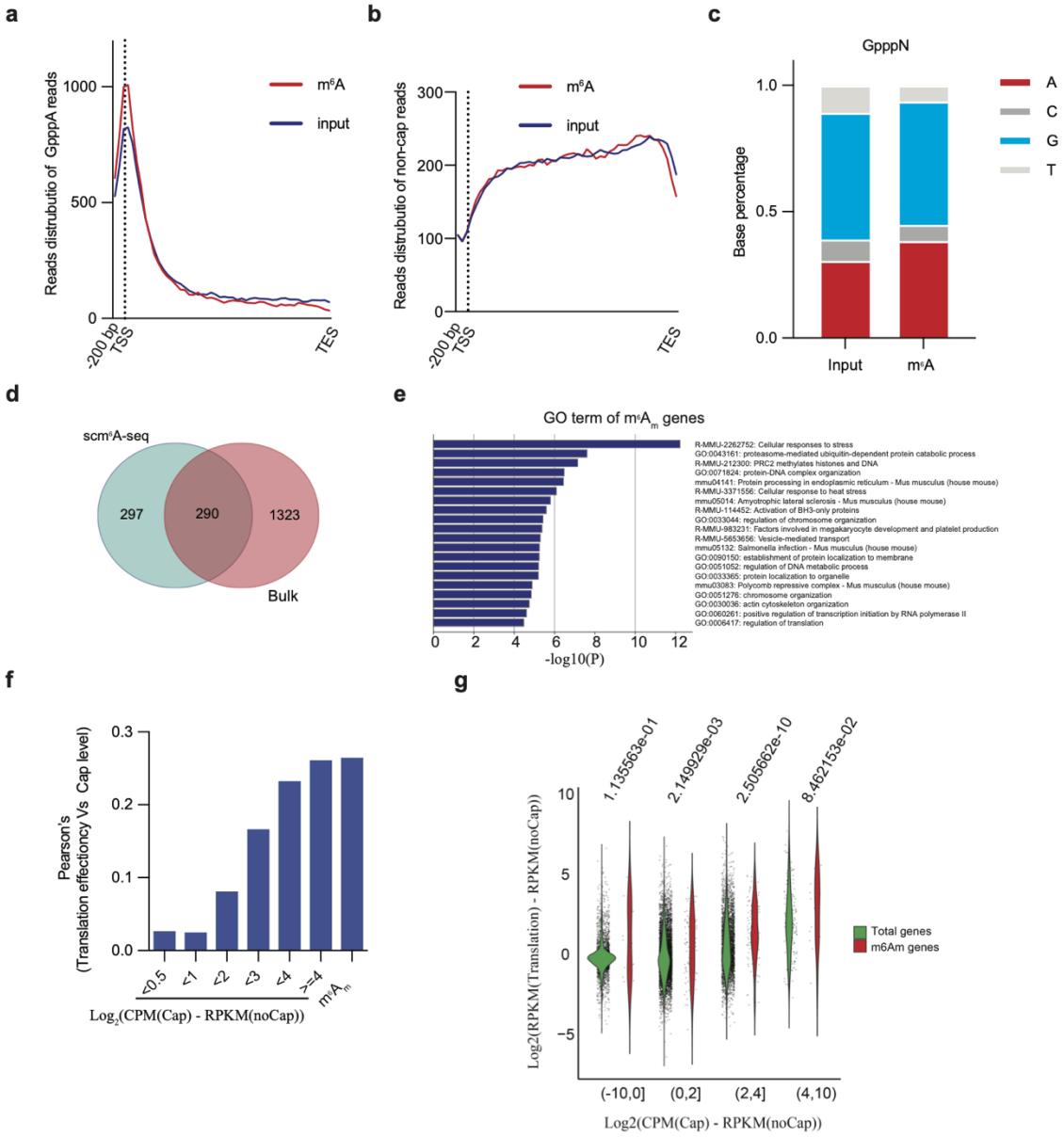

Figure 3| m^6A_m and m^7G cap improves maternal RNA translation in the oocytes. a-b Meta-gene plot showing the coverage distribution of m^7G cap reads (**a**) and non-cap reads (**b**) in input and m^6A-IP data sets. **c** The first base neat the m^7G cap in input and m^6A-IP data sets. **d** Venn plot showing the detected m^6A_m genes in scm^{6}A-seq data and bulk m^6A-seq data of mouse oocytes. **e** Go analysis result of the common m^6A_m genes of mouse oocytes. The analysis was performed using Metascape using default parameters. **f** Bar plot showing the correlation between translation and m^7G cap level. The gene sets were separated into different classes according to the m^7G cap level. **g** Violin plot showing the different translation efficiency between m6Am genes and other genes. The gene sets were separated into different classes according to the m^7G cap level. The two-sided P value was calculated by unpaired student t-test.

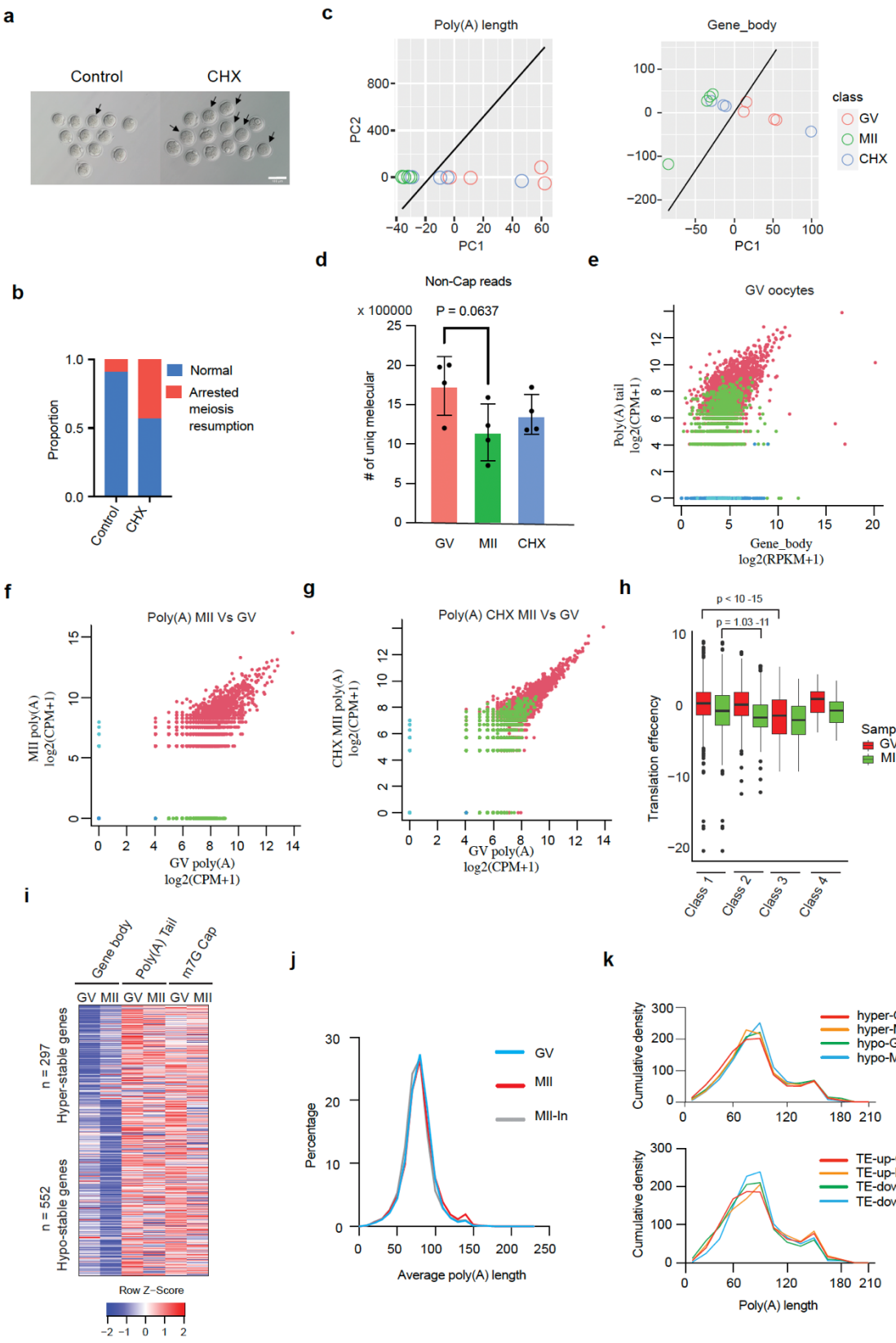
a
Control
CHX
b
Proportion
1.0
0.5
0.0
Normal
Arrested meiosis resumption
Control
CHX
c
Poly(A) length
PC2
PC1
Gene_body
class
GV
MII
CHX
d
Non-Cap reads
x 100000
P = 0.0637
# of uniq melecular
GV
MII
CHX
e
GV oocytes
Poly(A) tail log2(CPM+1)
Gene_body log2(RPKM+1)
f
Poly(A) MII Vs GV
MII poly(A) log2(CPM+1)
GV poly(A) log2(CPM+1)
g
Poly(A) CHX MII Vs GV
CHX MII poly(A) log2(CPM+1)
GV poly(A) log2(CPM+1)
h
p < 10 -15
p = 1.03 -11
Translation effecency
Sample
GV
MII
Class 1
Class 2
Class 3
Class 4
i
Gene body
Poly(A) Tail
m7G Cap
GV MII GV MII GV MII
n = 297
Hyper-stable genes
n = 552
Hypo-stable genes
Row Z-Score
j
Percentage
GV
MII
MII-In
Average poly(A) length
k
Cumulative density
hyper-GV
hyper-MII
hypo-GV
hypo-MII
TE-up-GV
TE-up-MII
TE-down-GV
TE-down-MII
Poly(A) length

Figure 4| Maternal RNA Poly(A)-tail structure regulates translation efficiency reshaping during oocyte maturation. **a** In vitro maturation (IVM) result of mouse oocytes in both the control (n=12) and CHX treated group (n=14), the arrested oocytes were labeled using black arrows. **b** Bar plot showing the proportion of cell types of IVM result. **c** Dot plot showing the PCA matrix of poly(A) length data (left) and gene body data (right) of GV oocytes, MII oocytes, and CHX-treated MII oocytes. The line shows the SVM decision function calculated using normal GV oocytes and MII oocytes. **d** Bar plot showing the non-cap (gene body) reads detected in the GV oocytes (n=4), MII oocytes (n=4), and CHX-treated MII oocytes (n=4). The two-sided P value was calculated by unpaired student t-test. **e-g** Dot plot showing the gene expression level of poly(A)ome expression level and gene body expression level in GV oocytes, the gene expression level of poly(A)ome in GV oocytes and MII oocytes (**f**) and the gene expression level of poly(A)ome in normal MII oocytes and MII oocytes treated with CHX (**g**). The different gene classes are colored in different colors. **h** Bar plot showing the translation efficiency of different gene sets in GV oocytes and MII oocytes. The two-sided P value was calculated by unpaired student t-test. **i** Heatmap showing the multi-omics expression level (gene-body, poly(A), m^7G) of hyper-stable genes and hypo-stable genes in GV oocytes and MII oocytes. **j** Density plot showing the distribution of poly(A) length in GV oocytes, MII oocytes, and CHX-treated MII oocytes. **k** Density plot showing the distribution of poly(A) length in different gene sets, the genes are classified according to RNA stability (upper) and translation efficiency (lower).

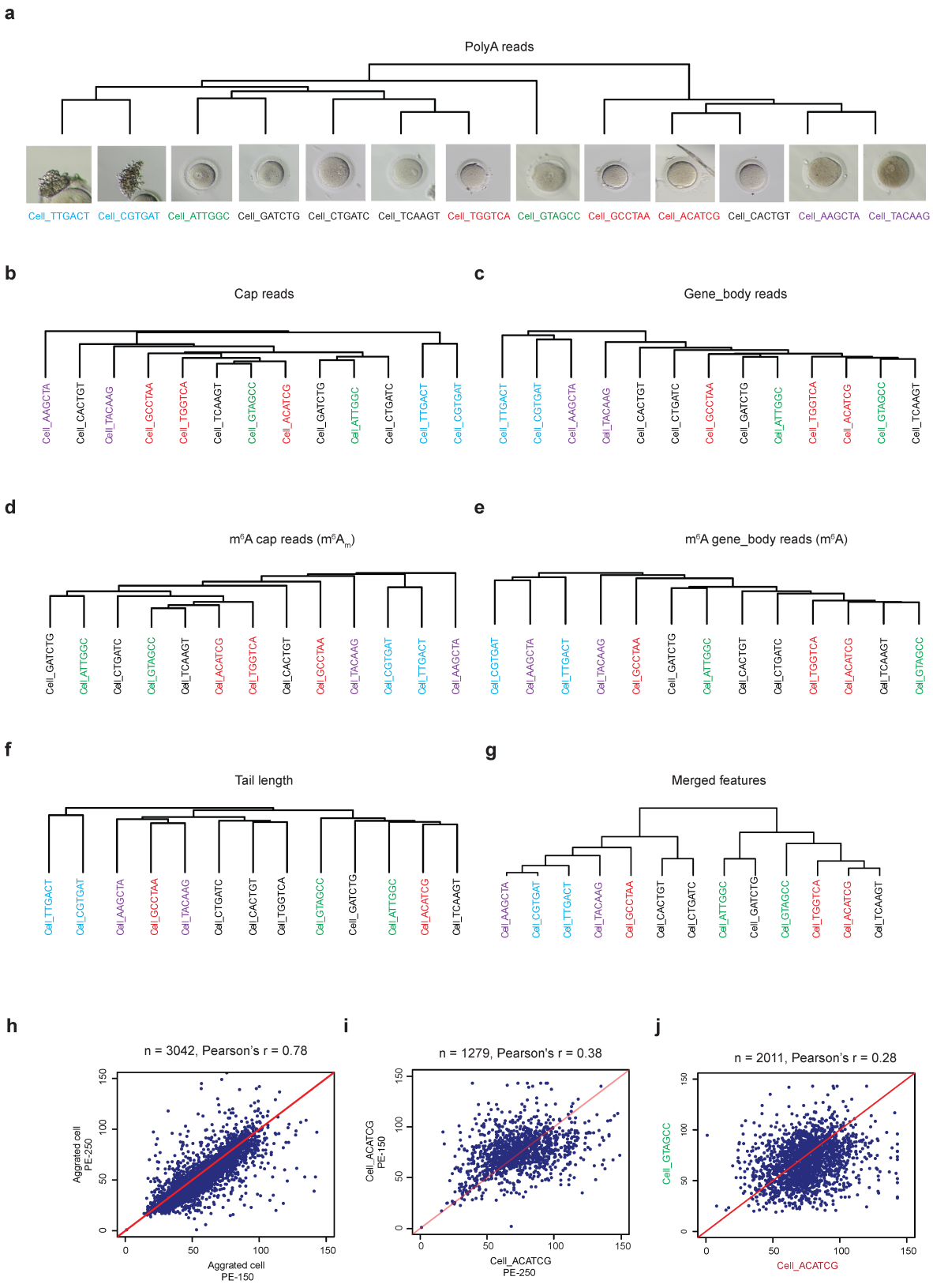
a
PolyA reads
Cell_TTGACT
Cell_CGTGAT
Cell_ATTGGC
Cell_GATCTG
Cell_CTGATC
Cell_TCAAGT
Cell_TGGTCA
Cell_GTAGCC
Cell_GCCTAA
Cell_ACATCG
Cell_CACTGT
Cell_AAGCTA
Cell_TACAAG
b
Cap reads
c
Gene_body reads
d
m6A cap reads (m6Am)
e
m6A gene_body reads (m6A)
f
Tail length
g
Merged features
h
n = 3042, Pearson's r = 0.78
Aggrated cell PE-250
Aggrated cell PE-150
i
n = 1279, Pearson's r = 0.38
Cell_ACATCG PE-150
Cell_ACATCG PE-250
j
n = 2011, Pearson's r = 0.28
Cell_GTAGCC
Cell_ACATCG

Figure 5| Maternal RNA Poly(A)-tail structure regulates translation efficiency reshaping during oocyte maturation. **a-g** Hierarchical clustering of single oocytes using the feature of poly(A) structure level (**a**), m^7G cap level (**b**), gene expression level (**c**), m^6A_m level (**d**), m^6A level (**e**), tail length (**f**) and merged PCA matrix data (**g**). **h-i** Dot plot showing the correlation between poly(A) tail length result of each gene calculated using the PE150 or PE250 data. Both aggregated data (**h**) and single-cell data (**i**) are shown. **j** Dot plot showing the correlation of poly(A) tail length result of each gene between different cells